Spring 5-19-2017

Aerodynamics and Vortex Structures of a Flapping Airfoil in Forward Flight in Proximity of Ground

Hang Li
Washington University in St. Louis

WASHINGTON UNIVERSITY IN ST. LOUIS

School of Engineering and Applied Science
Department of Mechanical Engineering and Material Science

Thesis Examination Committee:
Ramesh Agarwal, Chair
David A. Peters
Swami Karunamoorthy

Aerodynamics and Vortex Structures of a Flapping Airfoil in Forward Flight in Proximity of Ground

by
Hang Li

A thesis presented to the School of Engineering and Applied Science
Washington University in partial fulfillment of the
requirements for the degree
of Master of Science

May 2017
St. Louis, Missouri

Table of Contents

List of Figures

Acknowledgments

My deepest gratitude goes first and foremost to Prof. Ramesh K Agarwal, my supervisor, for his constant encouragement and guidance. Without his consistent and illuminating instructions, this thesis could not have reached its present form.

Second, I would like to express my heartfelt gratitude to Dr. Qu, who have instructed and helped me a lot in past one year. I also owe my sincere gratitude to my friends and my fellow classmates in CFD lab who gave me their help and time in listening to me and helping me work out my problems.

Finally my thanks would go to my beloved family for their loving considerations and great confidence in me all through these years.

Hang Li

Washington University in St. Louis

May 2017

Dedicated to my parents

ABSTRACT OF THE DISSERTATION

Aerodynamics and Vortex Structures of a Flapping Airfoil in

Forward Flight in Proximity of Ground

by

Hang Li

Master of Science in Mechanical Engineering

Washington University in St. Louis, 2017

Research Advisor: Professor Ramesh K Agarwal

The traditional flapping wing high lift mechanism research mainly focuses on the wing in unbounded flow. However, the real insect flight includes not only the unbounded flow field but also the near-surface flight. Therefore, research on near-surface flight can help reveal the high-lift mechanism of insect flight and should also be beneficial to the research on Micro-Air-Vehicles (MAV). In this thesis, the flow fields of an airfoil in hover and forward flight are simulated in the presence of ground by newly available function of "dynamic meshing" in ANSYS Fluent is employed. The characteristics of aerodynamics, pressure distribution, and vortex structure are analyzed. The vortex structure and aerodynamic characteristics in unbounded flow ($H/C=\infty$) are first analyzed in detail, three-typical vortex structure topologies are obtained, which are due to "translational forces," "rotational circulation," and "wake capture". By comparing the pressure coefficient and vortex structure around the airfoil at three typical moments during hover and forward flight in unbounded flow, the influence of incoming flow on vortex structure is analyzed and the reason for disappearance of high lift mechanism under certain condition is found.

As the height of airfoil decreases in ground effect, the first vortex pair near the airfoil begins to develop differently than that in unbounded flow (H/C = ∞) and the ground effect begins to appear slowly. The presence of the ground mainly restricts the descent of the vortex pair and influences the newly generated vortex at the leading and the trailing edge that have just separated from the airfoil. As the height of the airfoil further decreases, the trailing edge vortex in up stroke gradually moves to right side away from the airfoil, and this change in the vortex movement leads to disappearance of increased lift effect. In the forward flight, typical vortex structures due to “translational forces” and “rotational circulation” still exist. Due to incoming flow, the vortex generated at the leading and the trailing edge fall-off rapidly from the airfoil. Shedded vortices moving downstream with the incoming flow result in a complex vortex structure, which lead to the disappearance of “wake capture” vortex structure and lift enhancement in up stroke.

Chapter 1: Introduction

Insects remain unsurpassed in many aspects of aerodynamic performance and maneuverability. With appropriate kinematics, frequency and amplitude, flapping wing could generate substantially higher lift and perform well beyond the stall angle of attack of fixed wings. Several experiments have shown that the quasi-steady aerodynamic theory [1] is inadequate to explain the mechanism of high lift in flying insects, it is clear that unsteady aerodynamic theory [2] is needed to explain the insect flight. Sane and Dickinson have shown by experimental methods that delayed stall, rotational circulation, and wake capture [3, 4] are three characteristics observed in flapping wing flight.

Current research on insect flight has been focused on unbounded flow, while the actual insect flight includes both the unbounded and near-surface flight. Gao employed an immersed boundary-lattice Boltzmann method [5] to solve the two-dimensional incompressible Naiver-Stokes equations to explain the high lift mechanism of insects in ground effect. Gao analyzed the influence of phase difference and rotation amplitude on the near-surface aerodynamic characteristics of insects hovering in ground effect. Mao pointed out that the wake capture enhances [6] the leading-edge vortex and increases the aerodynamics forces on the insect near the ground.

Insect have many kinds of near ground flight, like dragon fly skimming the ground, the bee and the butterfly collecting nectar from the flowers, etc. At present, there are hardly any studies on insect forward flight in proximity of ground. Research on near surface forward flight of insects would enhance the understanding of their aerodynamics and helpful in the development of micro air vehicle.

Chapter 2: Computational Domain, Mesh Types and Boundary Conditions

The aerodynamics forces on an airfoil are obtained by integrating the pressure and the viscous shear stress on the surface of the airfoil. The airfoil surface pressure is typically an order of magnitude higher than the viscous shear stress, therefore the analysis of pressure distribution on the airfoil can provide a good measure of force change on the airfoil.

Figure 3.1 and Fig. 3.2 show the computational domain grid types and boundary conditions for a flapping airfoil in hover and in ground effect, respectively. Fig. 3.3 shows computational domain, mesh types and boundary conditions for a flapping airfoil in forward flight in ground effect. These figures show conformal structured grid around airfoil in (region 1) with 400 (circumferential) $\times$100 (radial) points, unstructured triangular mesh in the deformation zone (region 2) with total number mesh points close to 400,000 and the external unstructured grid (region 3) with 1000 (circumferential) $\times$100 (radial) points. The first layer of mesh height on the airfoil is $1.5 \times 10^{-4}C$ and time step is $\frac{1T}{32}$. At $\frac{H}{C} = \infty$, the number of grid points in the deformed area is twice that on the periphery.

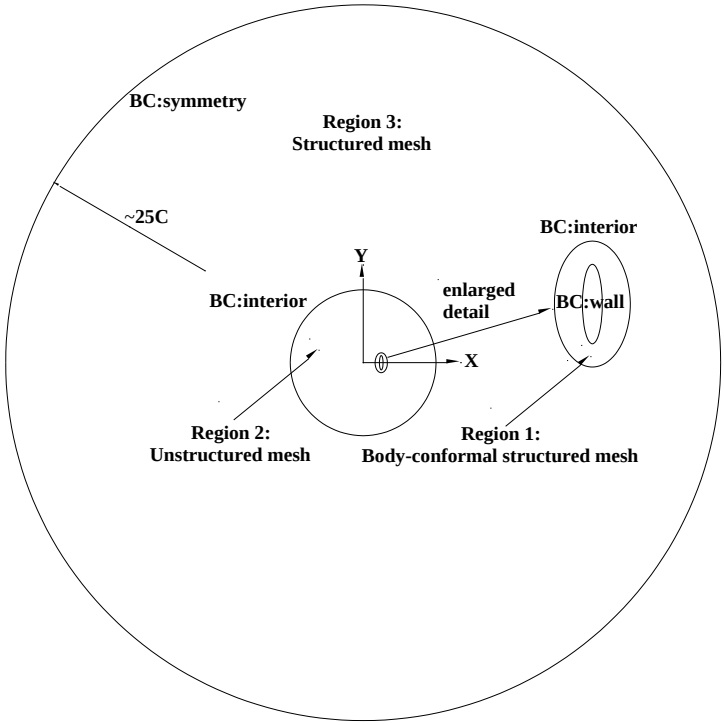

Figure 2.1 Computational domain, mesh types and boundary conditions in unbounded flow

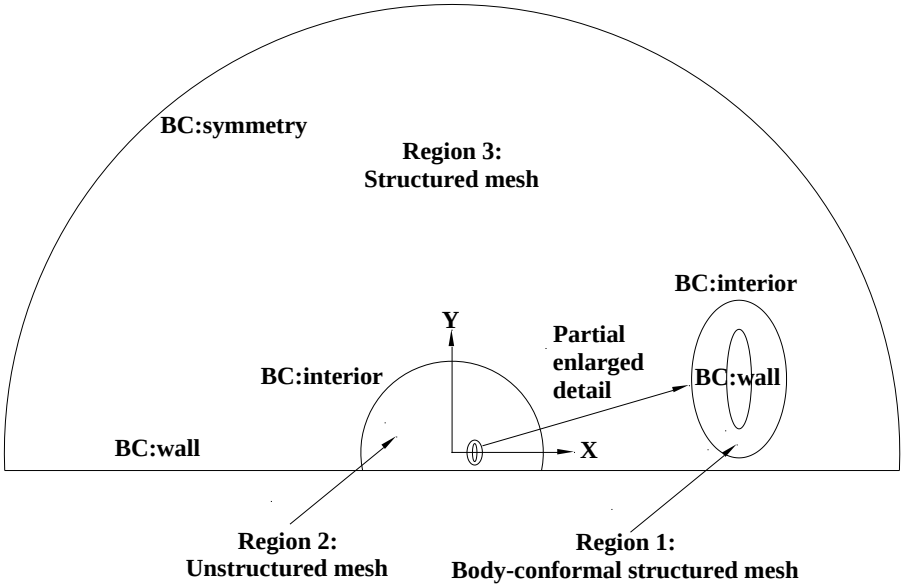

Figure 2.2 Computational domain, mesh types and boundary conditions in ground effect

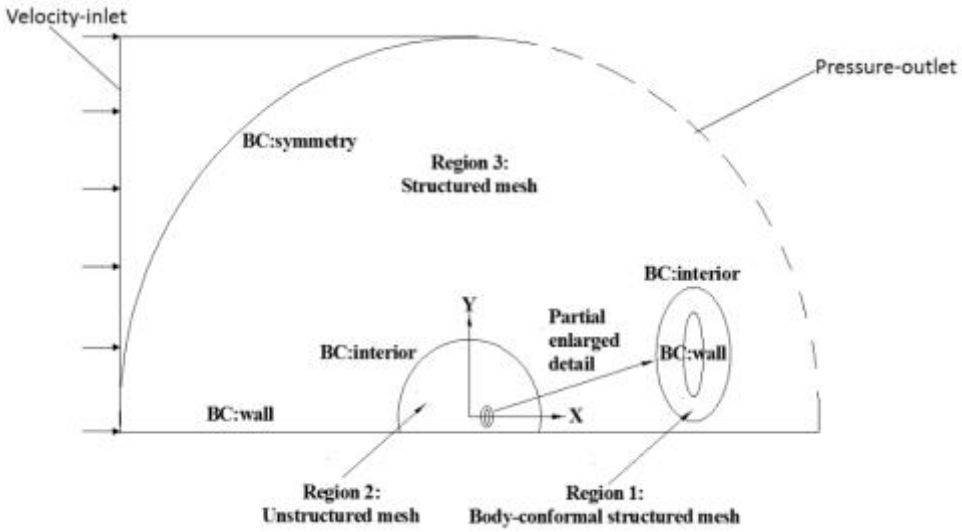

Figure 2.3 Computational domain, mesh types and boundary conditions in ground effect in forward flight

Chapter 3: Numerical Model

3.1 Equation of Motion of a Flapping Airfoil

In numerical simulation, unsteady incompressible Navies-Stokes equation are solved at low laminar flow Reynolds numbers for a flapping airfoil in unbounded flow and in ground effect both in hover and forward flight by employing the commercial CFD solver ANSYS Fluent V.17.1. Moving mesh method in Fluent is used and a UDF is written to describe the boundary conditions for the flapping airfoil. For the two-dimensional hovering motion of the flapping airfoil, the flapping plane is considered parallel to the ground. The slope of the airfoil is assumed to be elliptic. The equation of motion describing the flapping motion in hover are:

$$V_x = -2\pi A_m C \sin\left(\frac{2\pi t}{T}\right)/T \qquad (3.1)$$

$$\omega_z = 2\pi\alpha_m \cos\left(\frac{2\pi t}{T} + \phi\right)/T \qquad (3.2)$$

Where A_m is the amplitude of the translational motion measured as a multiple of the chord length, α_m is the amplitude of the rotation, C is the chord length, and T is the period of the motion. ϕ represents the phase difference between the rotational motion and the translational motion, which is taken to be zero. The coordinate system and the motion history sketch are shown in Fig. 2.1, where H represents the distance of center of rotation from the ground.

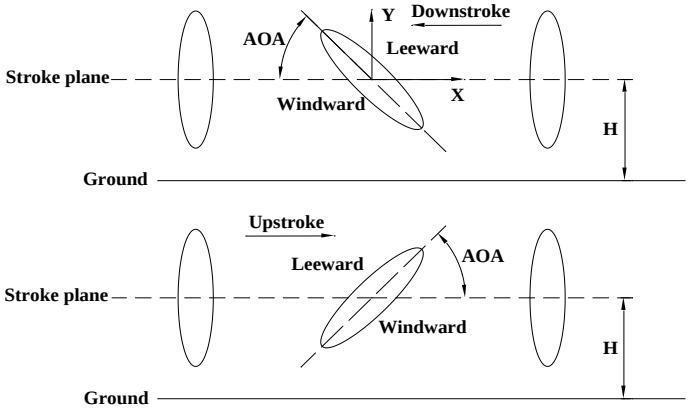

Figure 3.1 Schemetic diagram of a flapping airfoil in two strokes

3.2 Governing Equations of Fluid Dynamics

The governing equations of fluid dynamics can be written as:

Continuity equation:

$$\nabla \cdot \boldsymbol{U} = 0 \qquad (3.3)$$

Momentum equation:

$$\rho \frac{\partial \boldsymbol{U}}{\partial t} + \rho(\boldsymbol{U} \cdot \nabla)\boldsymbol{U} = -\nabla P + \rho F_b + \mu \nabla^2 \boldsymbol{U} \qquad (3.4)$$

Where U, ρ, t, P, F_b, μ are velocity, density, time, pressure, body force and dynamic viscosity.

SIMPLE algorithm in Fluent in employed for pressure-velocity coupling in Eq. (3.3) and Eq. (3.4). In Eq. (3.4), the second-order space discretization and first order time implicit discretization. The deformation of the fluid due to airfoil movement is described by the scalar whose conservation equation in integral form can be written as:

$$\frac{d}{dx}\int_V \rho\phi dV + \int_{\partial V} \rho\phi(\boldsymbol{U} - \boldsymbol{U_g})d\boldsymbol{A} = \int_V \Gamma \nabla\phi \cdot d\boldsymbol{A} + \int_V S_\phi dV \qquad (3.5)$$

Where $\boldsymbol{U_g}$ is the velocity of the grid, S is the source term and Γ is the diffusion coefficient. For the motion of the grid, we can write:

$$\boldsymbol{U}_{g,j} \cdot \boldsymbol{A}_j = \frac{\delta \boldsymbol{V}_j}{\Delta t} \qquad (3.6)$$

$$\frac{dV}{dt} = \int_{\partial V} \boldsymbol{U}_g dA = \sum_j^{n_f} \boldsymbol{U}_{g,j} \cdot \boldsymbol{A}_j \qquad (3.7)$$

$$\boldsymbol{V}^{n+1} - \boldsymbol{V}^n = \frac{d\boldsymbol{V}}{dt}\Delta t \qquad (3.8)$$

and

$$\frac{d}{dx}\int_V \rho\phi dV = \frac{(\rho\phi V)^{n+1} - (\rho\phi V)^n}{\Delta t} \qquad (3.9)$$

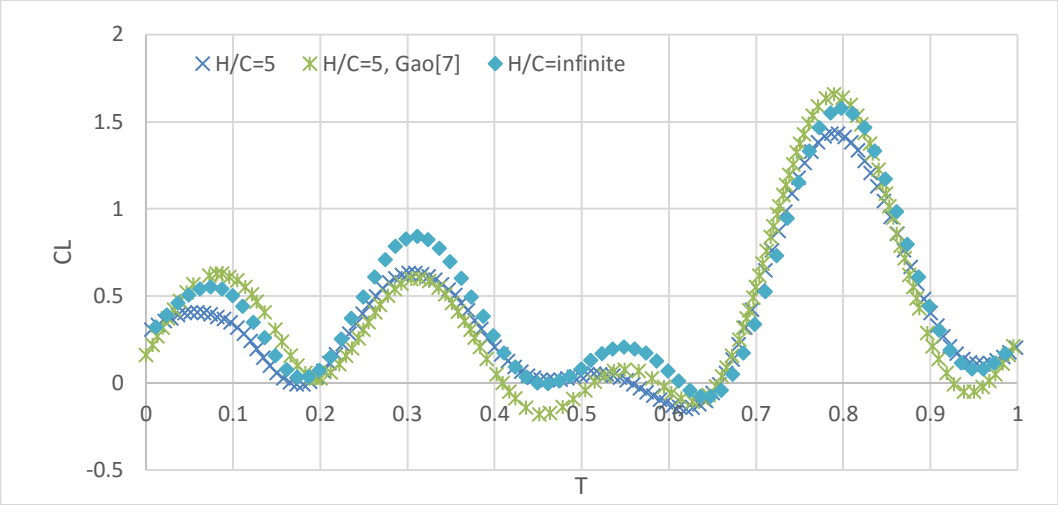

Figure 3.2 Variation in lift coefficient of a hovering flapping airfoil in ground height during one time period

3.3 Numerical Solution Validation

Gao [7] has deployed a numerical simulation of a flapping elliptical airfoil in hover in ground effect for $H/C = 5$ using the Immersed Boundary-Lattice-Boltzmann (IB-LBM) method. For validation of present solution methodology, computations were performed for the flow conditions of Gao. Fig. 3.4 shows the comparison of present computations for the variation of lift coefficient in time during one period for $H/C = 5$ and $H/C = \infty$ with those of Gao; Excellent agreement is obtained, if can be noticed that there is little different in the lift coefficient at $H/C = 5$ and $H/C = \infty$.

Chapter 4: Numerical Simulation of Flowfield of a Flapping Airfoil in Hover and Forward Flight in Unbounded Flow

4.1 Flow Field in Hover

Using the flapping airfoil boundary conditions described in Equation (3.1) and Equation (3.2), flow field in hover in calculated in unbounded flow and in ground effect.

Fig. 4.1, Fig. 4.2 respectively show the variation in lift coefficient and drag coefficient during one period at $\frac{H}{C} = 5$.

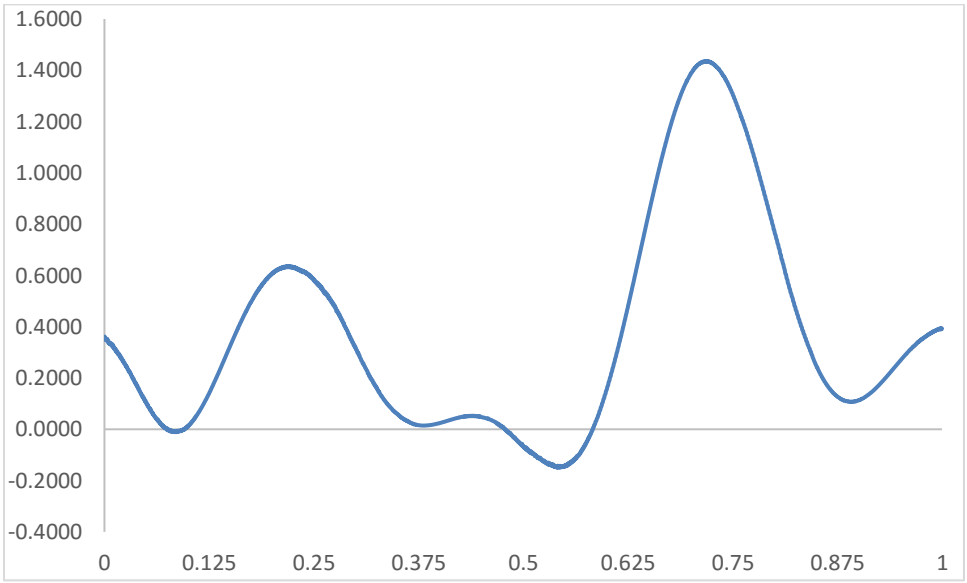

Figure 4.1 Variation in lift coefficient with time in hover at H/C=5

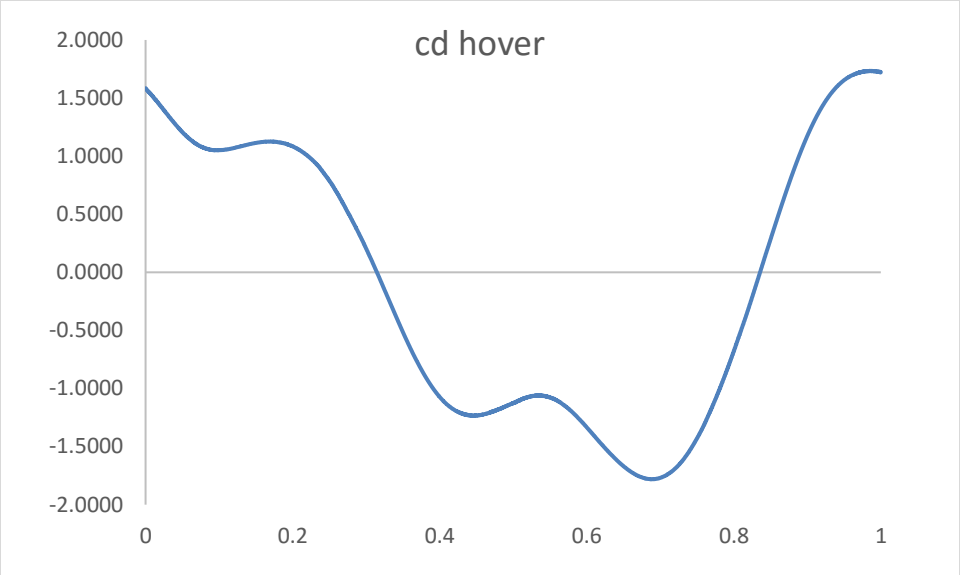

Figure 4.2 Variation in Drag coefficient with time in hover at H/C=5

In the following figures, the vortex structure and pressure distribution on the airfoil is shown. In Fig. 4.3, at t=1T/16, is the beginning of the down stroke, the airfoil is moving from right side to left side and is rotating anticlockwise at the same time. At this time, the acceleration in translational movement is the biggest. The leading edge and trailing edge of the airfoil rapidly produce a strong vortex. The lee side of the airfoil experience negative pressure. Since the angle of attack is high, the lift is not very large. The windward side of the airfoil has two asymmetrical vortices: LEV-0U and TEV-0U. These two vortices induce acceleration in the flow between them. Windward side of the airfoil now has positive pressure. The rotation fuses the leading and trailing edge vortices to form a co-moving dipole pair, which has an induced accelerating effect to the fluid between the two vortices.

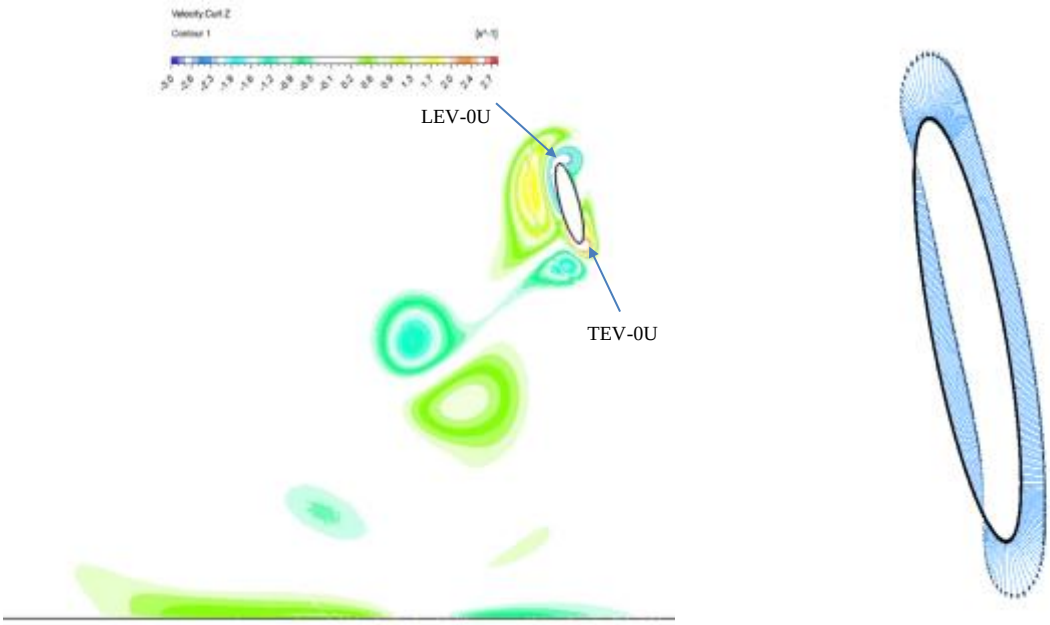

(a) (b)

Figure 4.3 Vortex structure and pressure coefficient of a flapping elliptic airfoil in hover at $t = \frac{1T}{16}$

As shown in Fig. 4.3, at 2T/16, leeward vortex in strength due to induction effect of the vortex on the windward side, thus the leeward side lift contribution is greatly increased (negative pressure increases). As the windward face vortex gradually moves away from the airfoil, the windward surface begins to form a single vortex structure. As the airfoil moves leftward, most of the vorticity gradually moves to the leeward side to create a down vortex. The existence of a single vortex structure induces negative pressure on the windward side and the positive pressure area on the windward surface is gradually reduced.

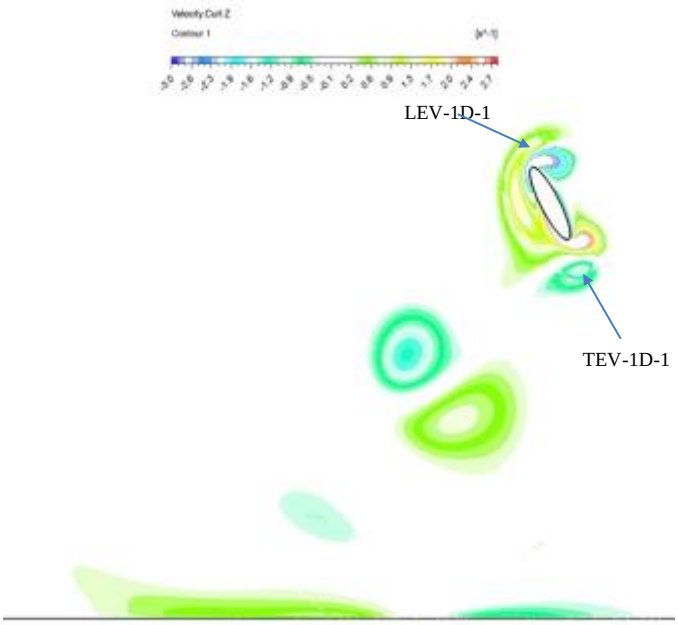

(a) (b)

Figure 4.4 Vortex structure and pressure coefficient of a flapping airfoil in hover at $t = \frac{2T}{16}$

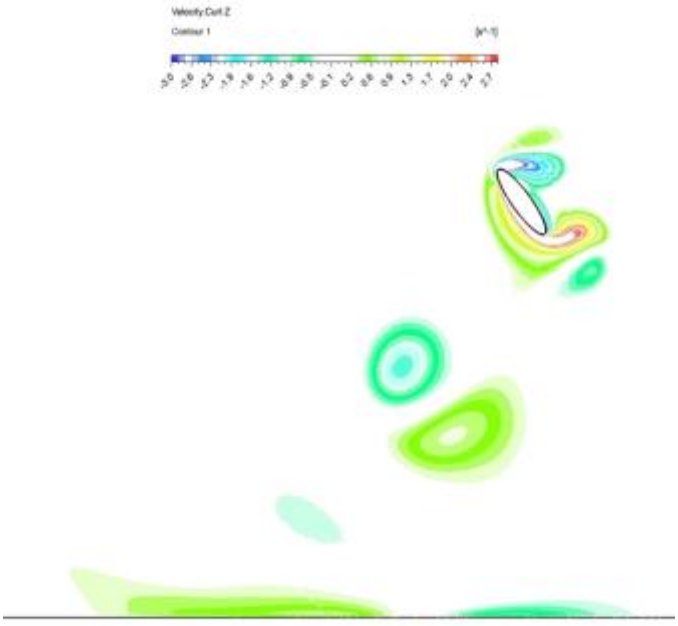

(a) (b)

Figure 4.5 Vortex structure and pressure coefficient of a flapping airfoil in hover at $t = \frac{3T}{16}$

As shown in Fig. 4.5 at t=3T/16, the windward vortex is gradually merging into the leeward vortex, as a result, the vortex-induced negative pressure on the windward surface becomes the stronger.

After complete merging of the windward vortex into leeward vortex as shown in Fig. 4.6 at t=4T/16, the leeward vortex begins to diffuse, the negative pressure on the leeward side is reduced, and the positive pressure area is gradually restored. At the same time, taking into account the angle of attack factors, the leeward lift at t=5T/16 reach as the maximum. After 5T/16, the up and down leeward vortex gradually fall off from the airfoil as the airfoil decelerates and rotates clockwise, and the positive and negative pressure zones also gradually changed. The LEV of the leeward surface begins to generate rapidly at the beginning of the down stroke, and the LEV induces the leading edge negative pressure. But the change in the negative pressure at the leading edge is small, and the lift of the leeward side is mainly affected by the angle of attack; the windward surface is affected by the angle of attack, but also by actual induction of counter rotating vortices and the impact of shedding from the airfoil.

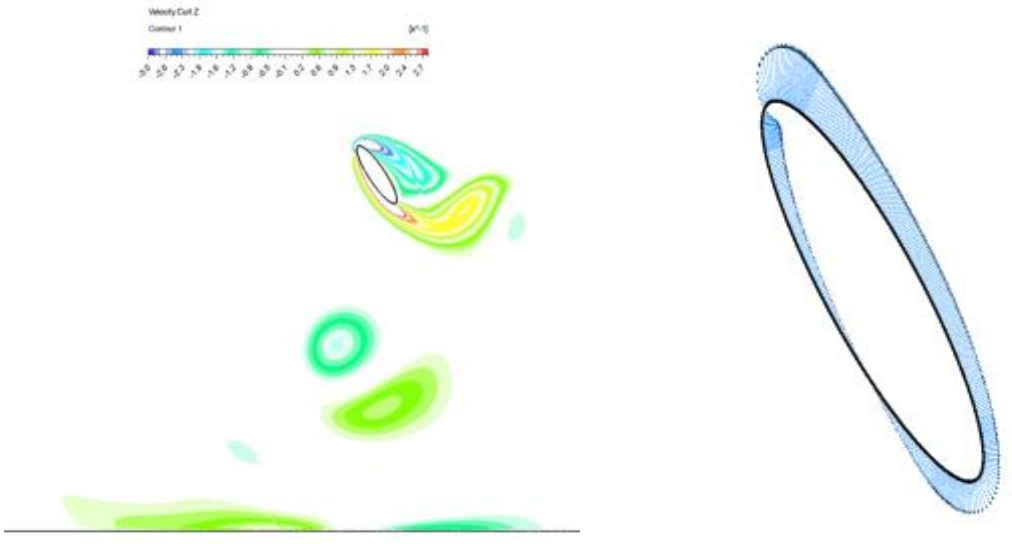

(a) (b)

Figure 4.6 Vortex structure and pressure coefficient of a flapping airfoil in hover at $t = \frac{4T}{16}$

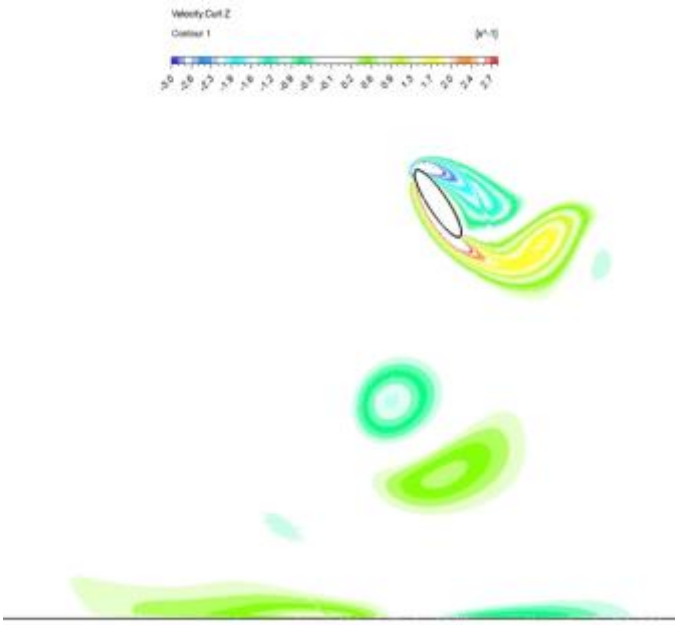

(a) (b)

Figure 4.7 Vortex structure and pressure coefficient of a flapping airfoil in hover at $t = \frac{5T}{16}$

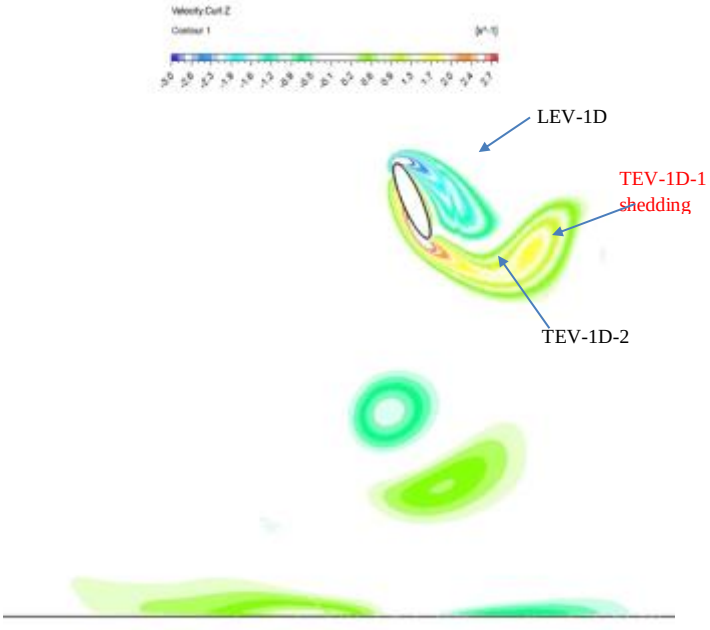

(a) (b)

Figure 4.8 Vortex structure and pressure coefficient of a flapping airfoil in hover at $t = \frac{6T}{16}$

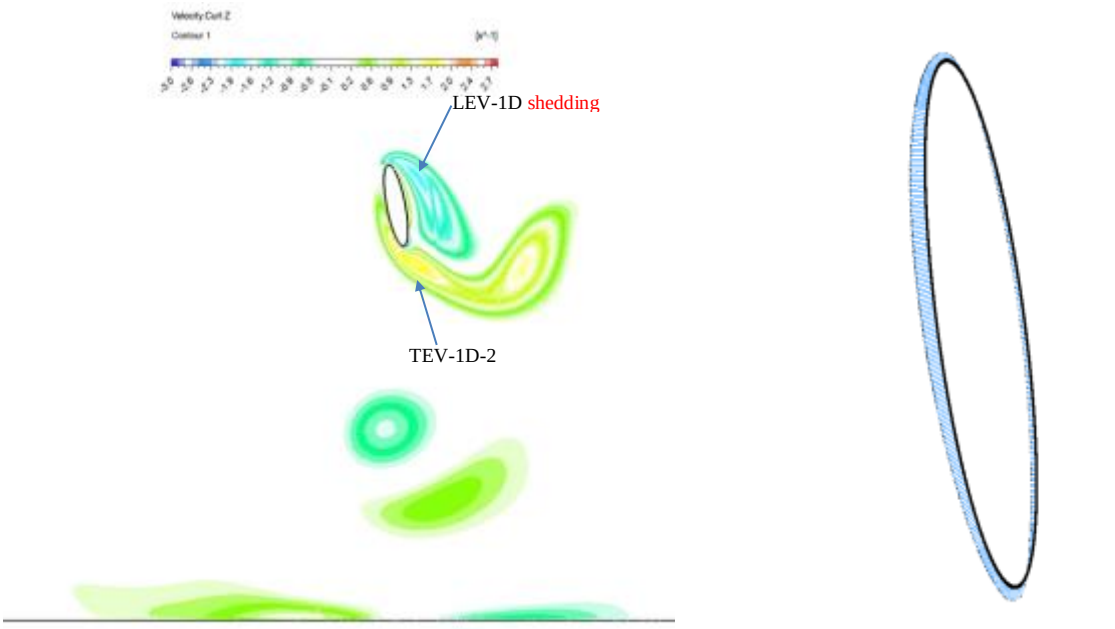

(a) (b)

Figure 4.9 Vortex Structure and pressure coefficient of a flapping airfoil in hover at $t = \frac{7T}{16}$

4.1.1 Summary of Flowfield in Down Stroke

In the down stroke, the LEV on the leeward surface begins to generate rapidly at the beginning of the stroke, and it induces negative pressure on the leading edge. However, the change in negative pressure at the leading edge is small, and the lift on the leeward side is mainly affected by the angle of attack; the lift on windward surface is affected by the angle of attack, but also by the acceleration flow created by the mutual induce of two counter rotating vortices (TEV-0U and LEV-0U) and the impact of shedding from the airfoil.

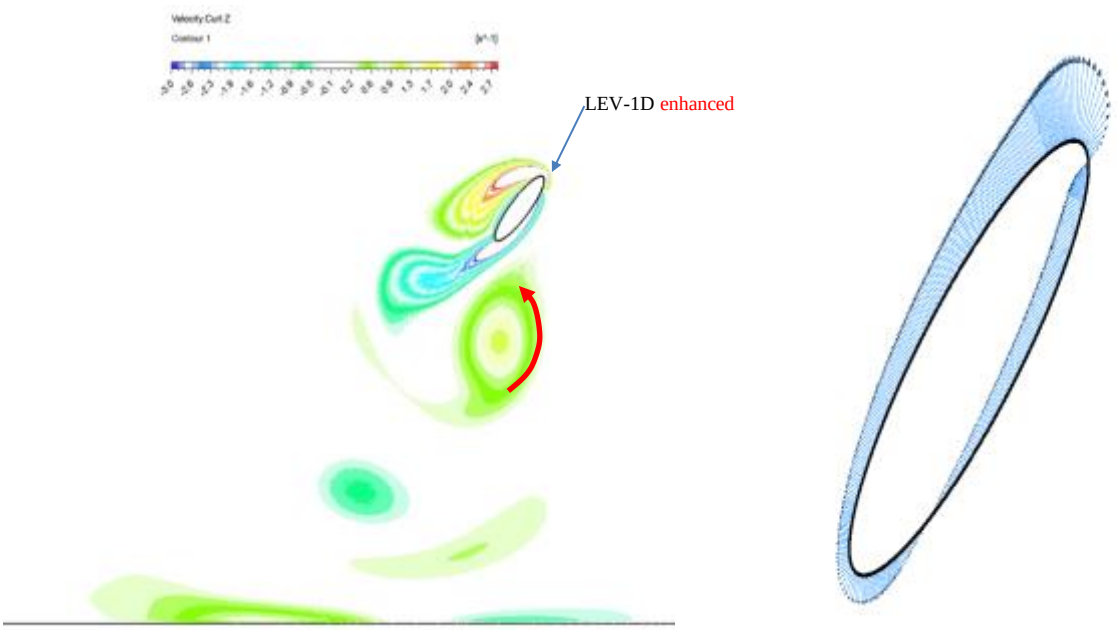

(a) (b)

Figure 4.10 Vortex structure and pressure coefficient of a flapping airfoil in hover at $t = \frac{13T}{16}$

4.1.2 Summary of Flowfield in Up Stroke

The difference in the flowfield in the down stroke and the upstroke is mainly due to the difference in the development of the trailing edge vortex. In the up-stroke, the airfoil passes through the TEV-1D-1 produced by the down stroke. During the down stroke, the presence of the vortex induced by LEV-1U formed upstroke, results in the negative pressure on the airfoil leeward surface larger than the absolute value of the corresponding pressure in first half-stroke at 5T/16, and the windward surface also experiences increases in the positive pressure because of its induced flow velocity is greater.

4.2 Discussion of Topologies of Typical Vortex Structures

Figure 4.11 shows the typical vortex structures various time. A, B, C, and D correspond to t=1T/16, 3T/16, 5T/16 and 13T/16, respectively.

In figure A, the airfoil translates to the left and rotates counterclockwise. The air strikes the windward surface and the windward surface forms a counter rotating double vortex structure. The double vortices induce acceleration of the fluid between them and create a large positive pressure area.

In figure B, the airfoil is translating to the left with counterclockwise rotation and the windward surface has a single vortex structure. This single vortex structure is very close to the airfoil to create the wind surface on the windward surface.

In figure C, the airfoil is translating to the left and begins clockwise rotation. A vortex is shed at the trailing edge and since the angle of attack reaches the minimum value, the overall lift performance of the airfoil is maximum.

In figure D, the airfoil translates to the right and rotates counterclockwise. The single vortex structure on the windward surface moves far away from the airfoil. It increases the velocity on the windward surface, enhances the LEV vortex strength and create a larger positive pressure. These phenomena have the effect of increase in lift.

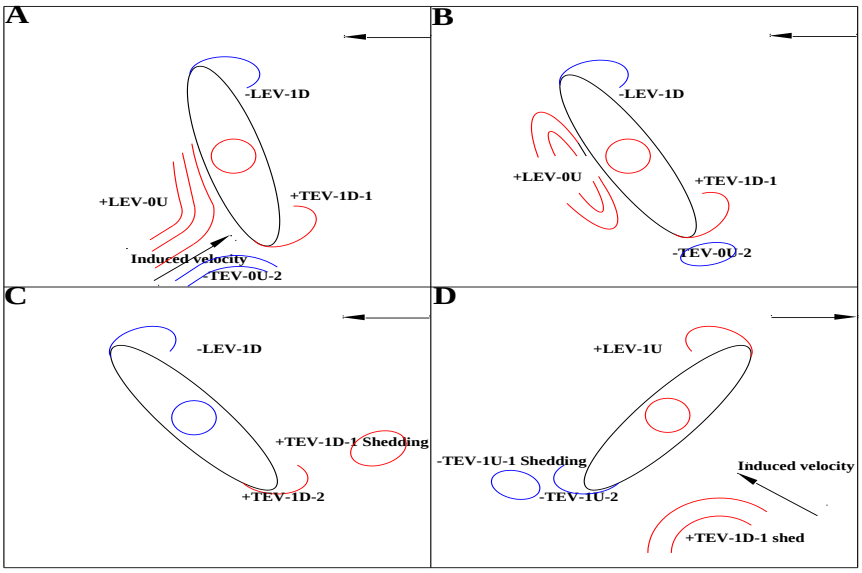

Figure 4.11 Typical Vortex Structures

4.3 Flowfield Analysis in Forward Flight

In Fig. 4.12 the variation of lift coefficient in forward flight in one period at H/C=5, one can observe two main characteristics: 1) the lift coefficient has a major period with many small period. 2) during the up stroke the lift is positive and in down stroke it is negative. In Fig. 4.13, from the variation in drag coefficient in forward flight in one period at H/C=5, one can observe that the drag coefficient also has a major period with many small periods, however its behavior in both the upstroke and down stroke is quite similar in contrast to that of the lift coefficient.

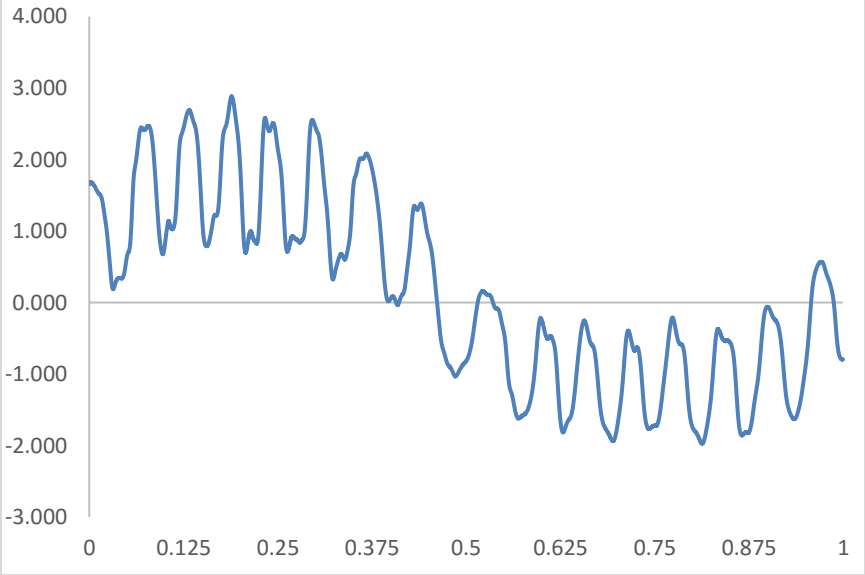

Figure 4.12 Variation of lift coefficient in time in forward flight at H/C=5

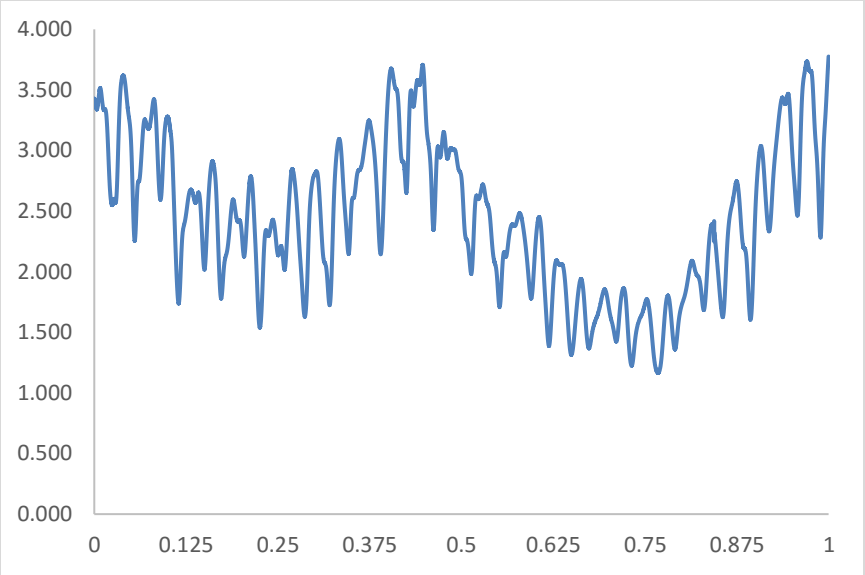

Figure 4.13 Variation of lift coefficient in time in forward flight at H/C=5

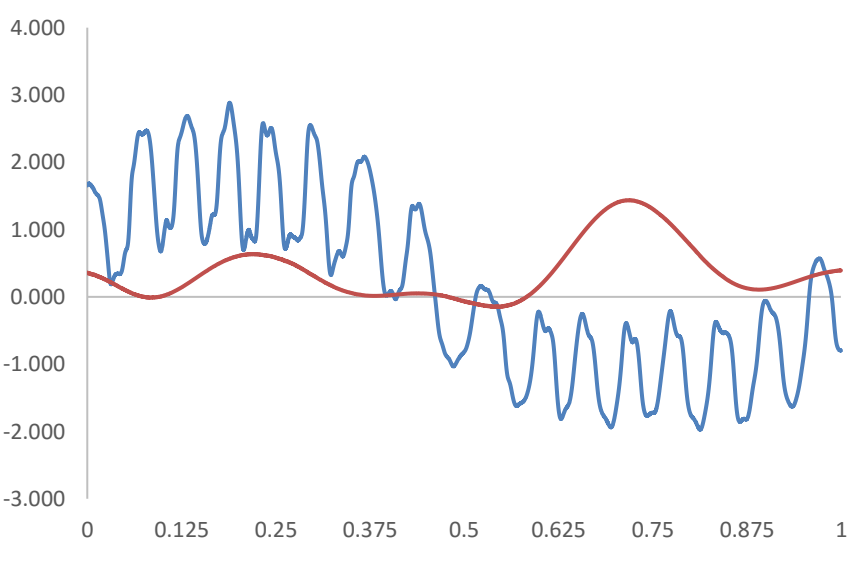

Figure 4.14 Comparison of lift coefficient in hover and forward flight at H/C=5

Fig. 4.14 shows the comparison of lift coefficient in hover and forward fight during one time period as H/C=5. It can be observed that there is only one major period in hover with smaller magnitude of lift coefficient. In Fig. 4.15, at t=1T/16, it is the beginning of the down stroke, the airfoil is moving from right to left and rotating anticlockwise at the same time. At this time, the

acceleration of the translational movement is the highest. The leading edge and trailing edge rapidly produce a strong vortex sheet.

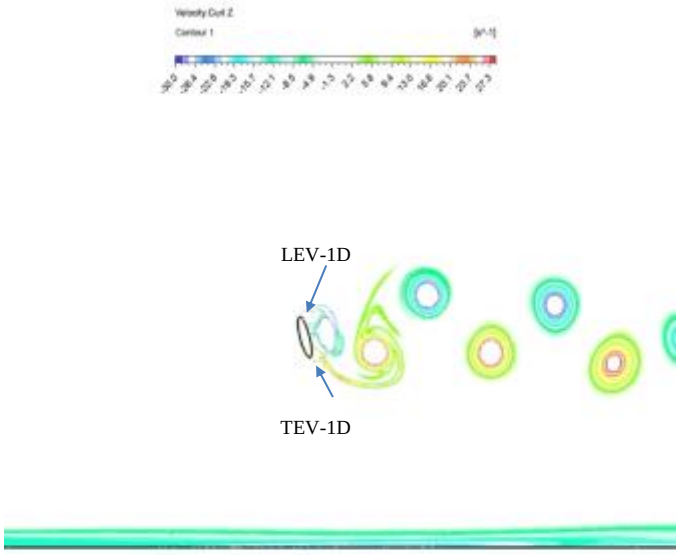

Figure 4.15 Vortex structure in forward flight for H/C=5 at $t = \frac{1T}{16}$

After 0.001s, these two newly generated vortex LEV-1D and TEV-1D would begin to strengthen and quickly become too strong for air to remain attached to the airfoil and thus rapidly shed from the airfoil. The effect of these two vortices on lift enhancement is similar to the two vortices in hover. These two vortices induce the acceleration in the flow between them and the lee side of the airfoil experiences negative pressure. Because of large angle of attack, lift is small. Windward side of the foil has positive pressure. The phenomenon of alternatively generating vortices and their shedding from the airfoil leads to fluctuation in the lift, which correspond to the peak and troughs in the lift coefficients.

In Fig. 4.16 at t=2T/16, the angle of attack is decreasing relative to the position at t=1T/16, thus the lee side of the airfoil has higher negative pressure, which increase the contribution to the lift from the airfoil. Comparing to the hover case at the same time, there is no "one single vortex

LEV-0U" attached to windward side of the airfoil due to the effect of the incoming flow. Thus, the positive pressure is still large at this time.

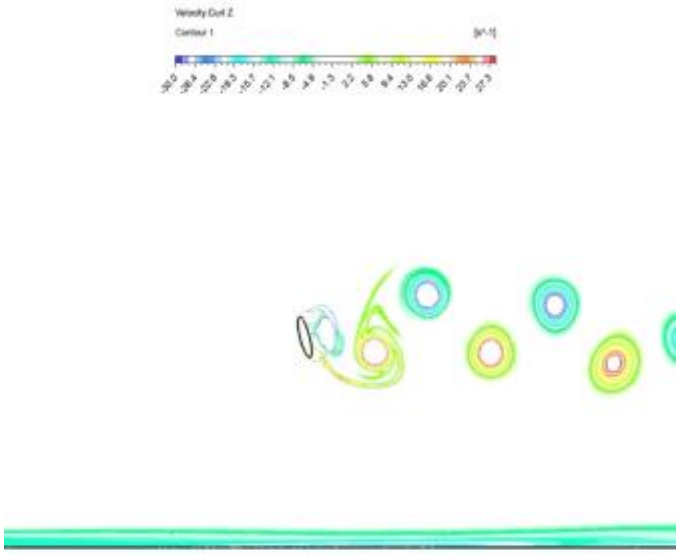

Figure 4.16 Vortex structure in forward flight for H/C=5 at $t = \frac{2T}{16}$

From t=3T/16 to 8T/16, the angle of attack first decreases and then increases to 90 degree. Considering the effect of angle of attack, it turns out that at t=5T/16 the lift of the airfoil reach a maximum.

Thus, during down stroke, the lift coefficient mainly depends on the angle of attack and the flow field fluctuation due to the vortex generation and shedding alternatively.

As shown in Fig. 4.17, at t= 9T/16 the direction of the flow is the same as the direction of the airfoil movement and therefore the lift is negative. At t=13T/16, the lift becomes lowest due to the angle of attack becoming the largest. Comparing with the hover case, in forward flight, the airfoil does not go through the vortex formed during down stroke. Therefore, the enhancement in lift due to the vortex is negligible.

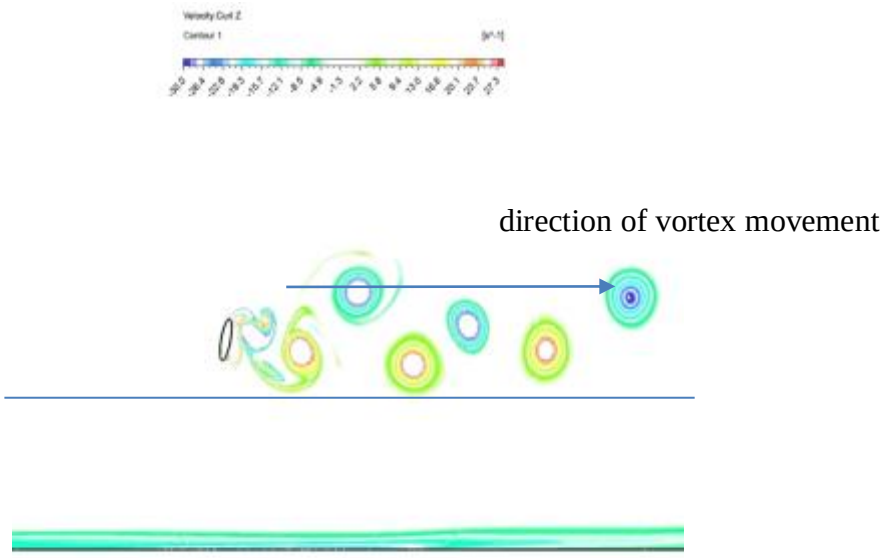

Figure 4.17 Vortex structure in forward flight for H/C=5 at $t = \frac{9T}{16}$

In order to explain the change in aerodynamic forces, in Fig. 4.18, the vorticity diagram at four typical instances of time for airfoil in hover and forward flight for a ground height H/C=5 are explained. The difference between forward flight and hover is mainly due to the influence of the incoming on the vortex structure near the airfoil and movement of the trajectory of the shed vortices. In forward flight, the number of the vortices shed increases and the movement of shed vortices is in streamwise direction instead of down ward towards the ground. Thus the "wake capture effect" disappears.

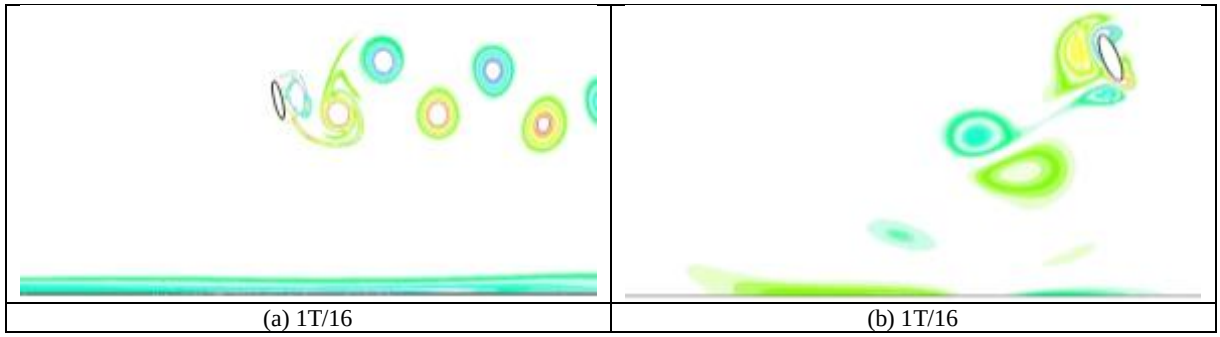

(a) 1T/16 | (b) 1T/16

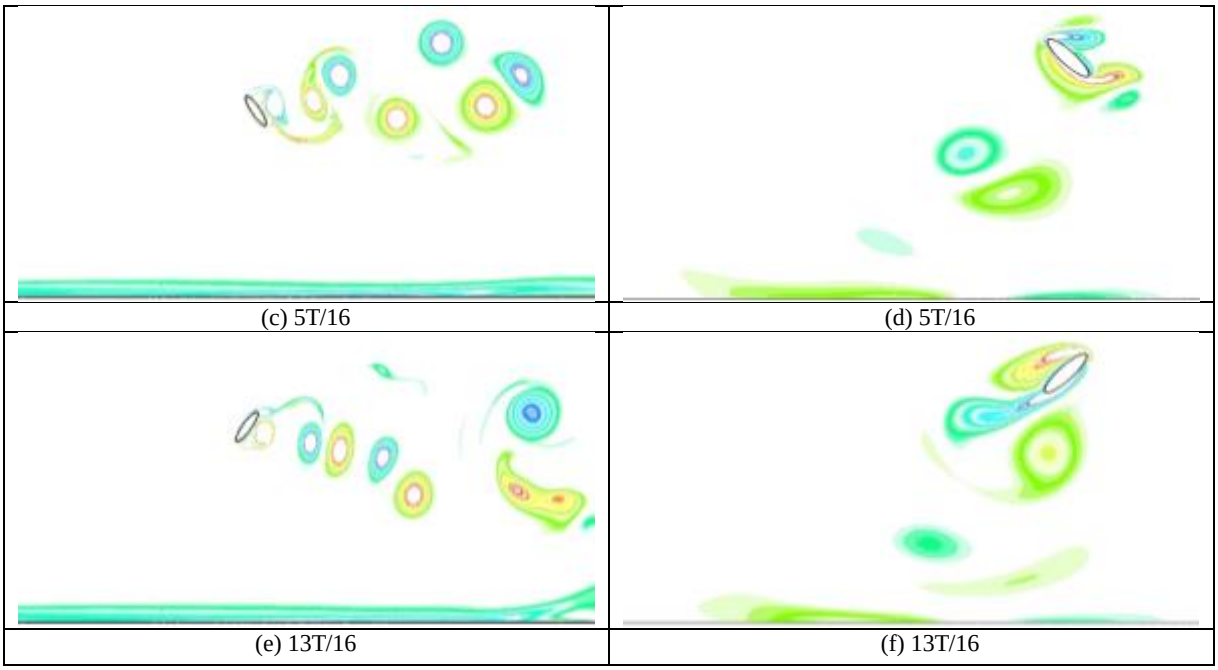

(c) 5T/16	(d) 5T/16
(e) 13T/16	(f) 13T/16

Figure 4.18 Comparison of vorticity contours at different time in hover and forward flight

Comparing the hover and forward flight at H/C=5 at the same instant in time, the movement of shed vortex in forward flight is in streamwise direction instead of downward to the ground. At t=1T/16, it is the beginning of the down stroke, the airfoil is moving from right side to left side and is rotating anticlockwise at the same time. The leading edge and trailing edge quickly form a strong vortex sheet due to the incoming flow and the airfoil accelerates to the left side. The lee side of the airfoil at trailing edge has negative pressure. Because of high angle of attack, the lift is not large. The windward side of the airfoil has positive pressure and the windward side of the airfoil has no vortex near it because of the incoming flow. Thus, the phenomenon of vortex pair induced acceleration of flow between them does not occur.

4.4 Conclusion

During one minor cycle the lift coefficient in one period in Fig. 4.12, the lift first increases due to the LEV enhancement and then decreases due to LEV shedding from the airfoil and due to the suction force at the trailing edge by newly formed TEV. The vortex shedding results in the

fluctuation in lift coefficient. The lift varies in down stroke basically due to change in angle of attack which first decreases and then increases. The lift reaches maximum at around t=5T/16 when the angle of attack is minimum.

In Fig. 4.11 A and B show the time of maximum lift and minimum lift respectively in one minor cycle. In Fig. 4.12 in A and B, the two newly generated vortex LEV-1D and TEV-1D begin to strengthen and quickly become strong for the airfoil to hold and thus are quickly shed from the airfoil. As shown in Fig. 4.12(A), when the LEV-1D is generated at the leading edge, the leeward side of the airfoil experiences a big suction force. As shown in Fig. 4.12 (B) moment, as LEV-1D further strengthens the trailing edge of the airfoil begins to generate a new vortex TEV-1D. Then the lift coefficient of the airfoil at the leading-edge decreases and the suction force at the trailing edge results in decreases in the lift. The multiple vortex shedding in a small period lead to fluctuation in lift. The major cycle of variation in lift coefficient is during a period consist of many minor cycles as shown in Fig. 4.12.

The vortex structure due to translational forces increases the lift, a typical vortex structure due to translational forces is shown in Fig. 4.11(A). The vortex structure due to rotational circulation shown in Fig. 4.11(B) has no single vortex on the windward side of the airfoil, thus the positive pressure on the windward side of the airfoil does not decrease. Rotational circulation results in increase in lift. However, the wake capture effect does not occur happen due to effect of incoming flow.

Chapter 5: Flapping Elliptic Airfoil in Ground Effect

When insects hover near the ground, their aerodynamic characteristics namely the pressure distribution, velocity and vorticity distribution will change due to the presence of ground. The research on this problem is of great significance in the design of the Micro-Air-Vehicles(MAV).

Figure 5.1 Variation in lift coefficients with time for a flapping airfoil in hover at different heights above the ground

5.1 Flapping Airfoil in Hover

Fig. 5.1 shows the variation in lift coefficients with time for the flapping airfoil in hover at different heights above the ground. This figure shows that biggest change in lift occurs at t=5T/16 and t=13T/16. Also, the average lift during the period decrease as the distance from the ground decreases.

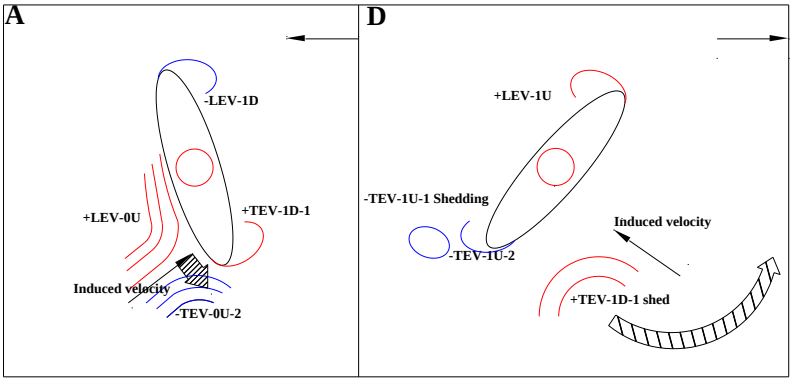

Figure 5.2 Typical vortex structures at t=1T/16 and (B) t=13T/16

In order to illustrate the changes in the aerodynamic force, the pressure distribution and the vorticity diagram are compared at t=5T/16 and t=13T/16 at different heights. The vortex structure of main interest is for conditions A and D in Fig. 5.2.

It can be seen from Fig. 5.2 that at H/C = 5, the double vortex structures TEV-0U-1 and TEV-0D-1 in the previous stroke are not affected by the ground in the next stroke. In addition, since the ground is still far away from the airfoil and the double vortex structure in the downward movement process gradually dissipates and therefore is able to induce only a weak shear layer on the ground. The vortex structures A and D at H/C=5 shown in Fig. 5.3 have little difference from that at H/C=∞.

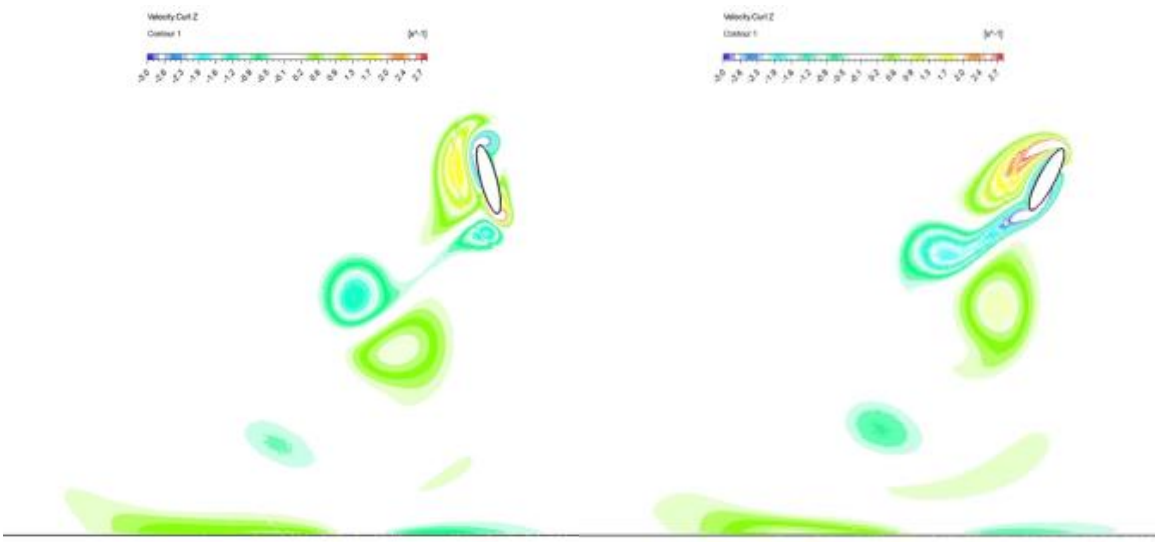

(A) (D)

Figure 5.3 Vortex structure A and D at H/C=5

At H / C = 3, the double-vortex structure of the previous stroke is squeezed by the ground. Since these two vortices are away from the trajectory of the airfoil, only TEV-0U-2 moves slightly downward and the other induction effects are very small as shown in Fig. 5.4. In the up stroke, for vortex structure D shown in Fig. 5.4. Vortex TEV-1D-1 is drifted to the right due to the influence of the ground shear layer resulting in a slight decrease in the induced flow acceleration and a slight decrease in the lift.

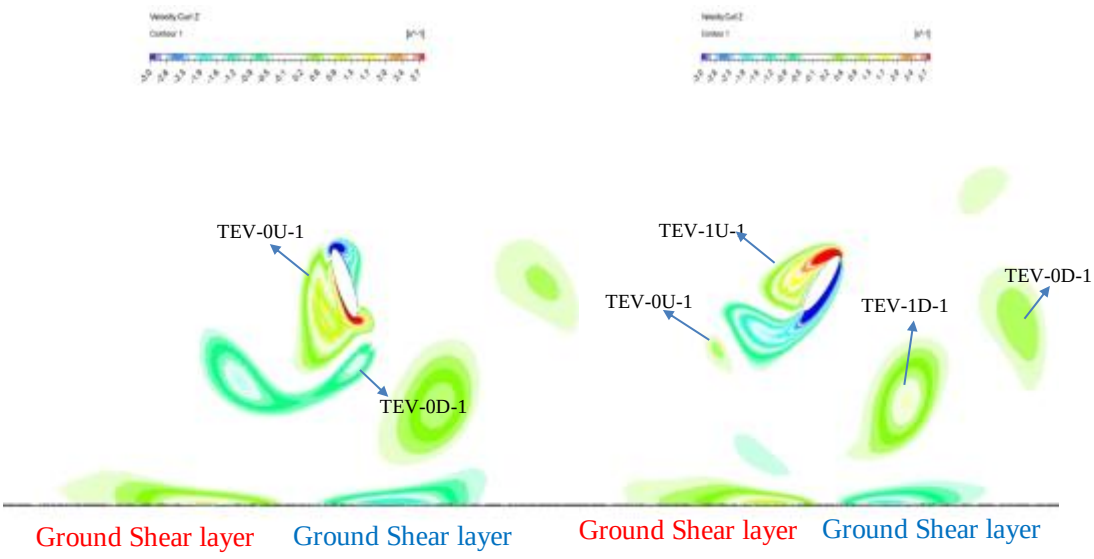

(A) (D)

Figure 5.4 Vortex structure of A and D at H/C=3

Fig. 5.4 shows the vorticity diagram at H/C=3. It can be seen from this figure that the TEV-1D-1 is induced to move to the right of the airfoil away from the airfoil. Therefore, the aerodynamic force in the down stroke is basically the same as the aerodynamic force in the up stroke.

The TEV-1D/1U-2, which falls off from the airfoil is finally squeezed into the shear layer due to the narrowing of the ground and the airfoil. This phenomenon contributes to the development of the ground shear layer at smaller H/C.

With decrease in the height of the airfoil from the ground, the effect of the ground due to obstruction of the fluid around the airfoil increases, which directly affects the vortex structure on the airfoil surface. Since the effect of the shear layer on the ground promotes the rightward movement of TEV-1D-1, the airfoil does not pass through the vortex.

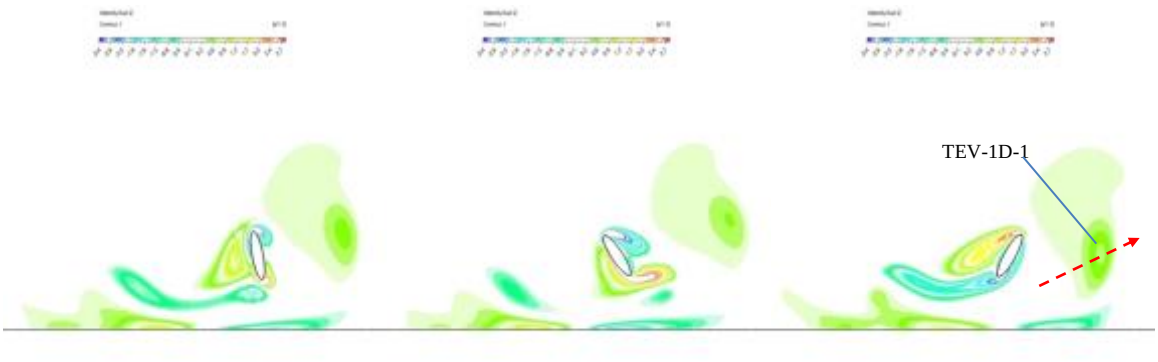

Figure 5.5 Vortex structures A, B and D at H/C=1 for ground effect in forward flight

5.2 Flapping Airfoil in Forward Flight

This section discusses the effect of ground on a flapping airfoil in forward flight. Fig. 5.6 shows the variation in lift coefficient with time during one period in hover and forward flight at H/C=1.5. Fig. 5.7 shows one peak and one trough in lift coefficient in one minor period of 1s in forward flight.

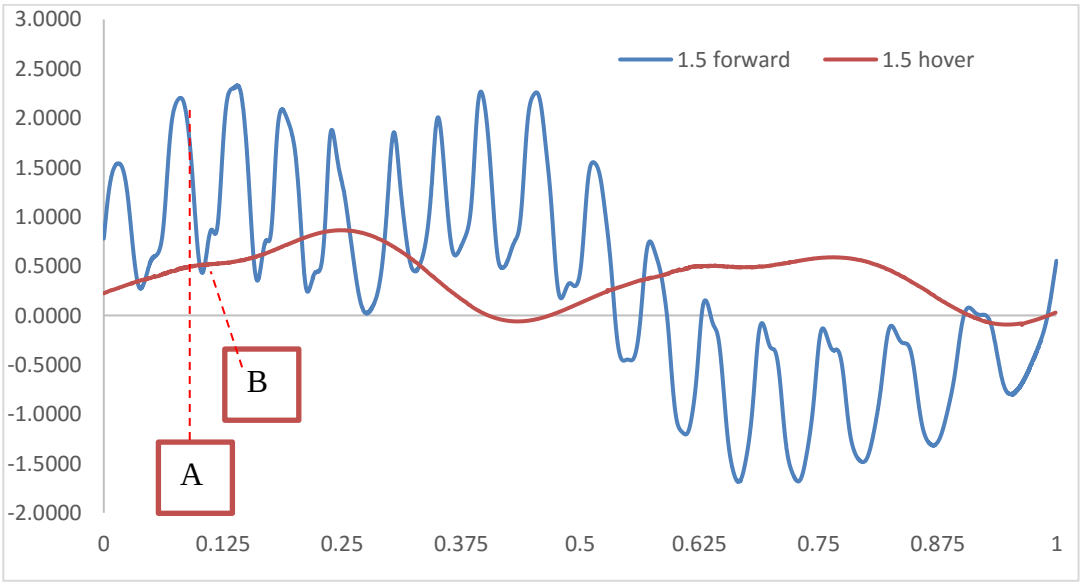

Figure 5.6 Variation in lift coefficient with time during one period in hover and forward flight at H/C=1.5

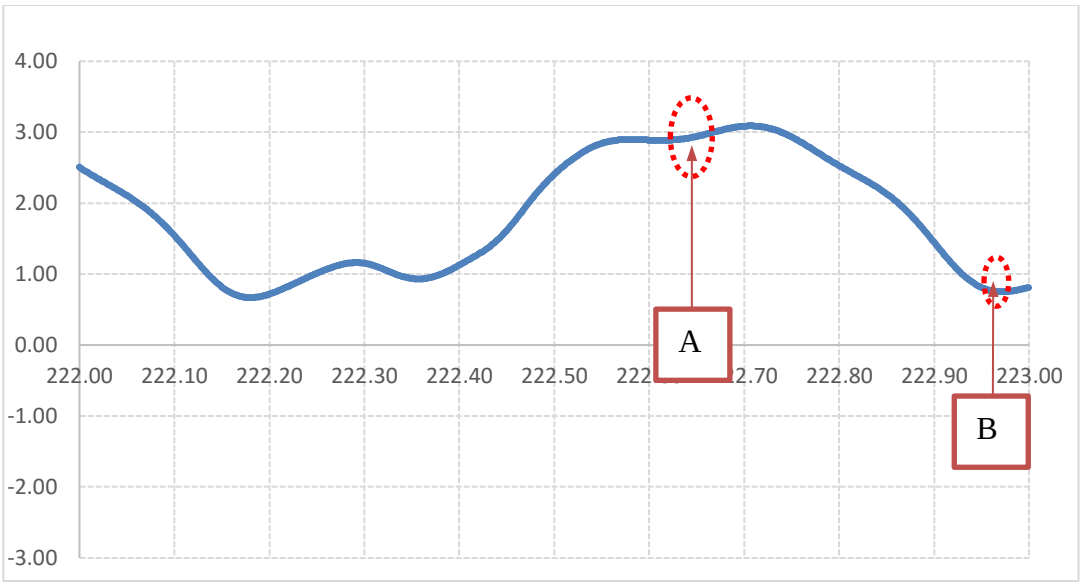

Figure 5.7 One peak and one trough in lift coefficient during one second of one minor period in forward flight

From the lift coefficient in Fig. 5.6 and Fig. 5.7, it can be seen that the lift has a major period and minor periods. During the up stroke the lift is positive and during the down stroke it is negative. This behavior of the lift phenomenon is quite the same with H/C=5 in forward flight as shown in Fig. 5.8.

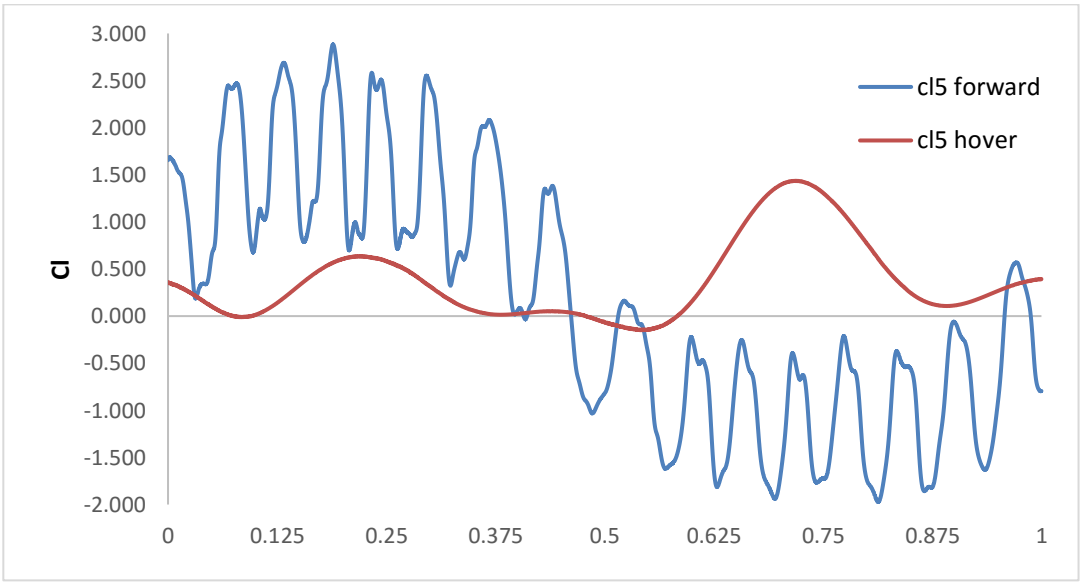

Figure 5.8 Variation in lift coefficient with time during one period in hover and forward flight at H/C=5

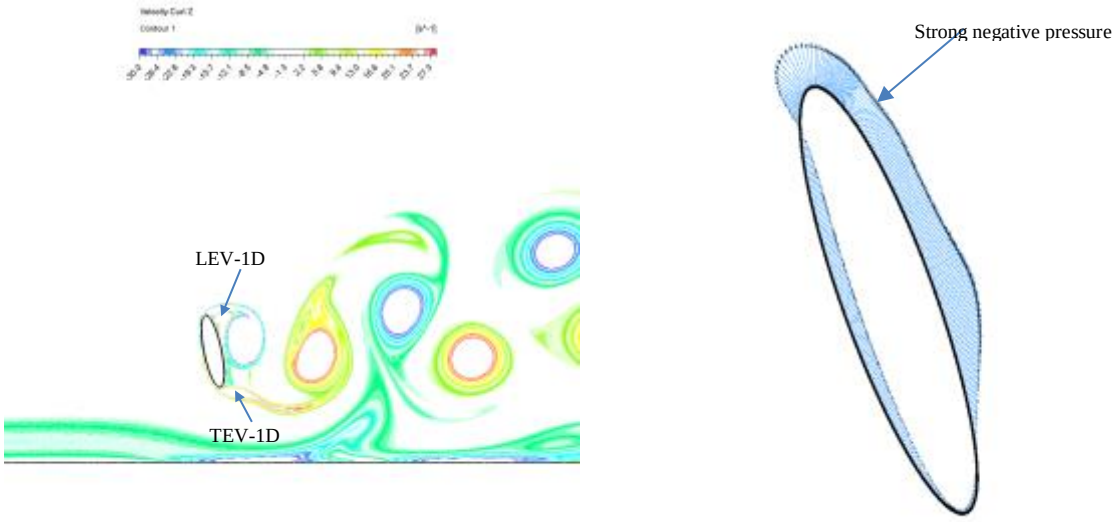

(a) (b)

Figure 5.9 (a) Vortex structure in forward flight and (b) pressure coefficient around the airfoil at H/C=1.5

Fig. 5.9 shows the vortex structure and pressure coefficient distribution around the airfoil at 0.5 sec in forward flight at H/C=1.5.

After 0.5s the two newly generated vortices LEV-1D and TEV-1D first strengthen and then quickly become too strong for the airfoil to hold and therefore quickly shed from the airfoil. Fig. 5.10 shows the pressure coefficient distribution around the airfoil at moment A and B in Fig. 4.11.

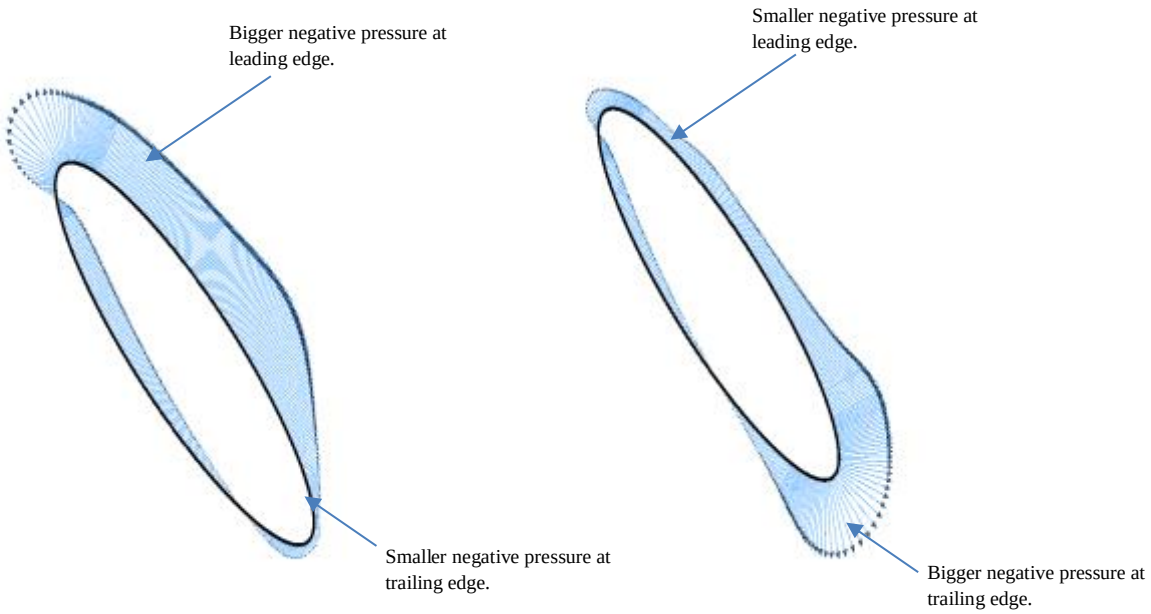

(A) (B)

Figure 5.10 Pressure coefficient around the airfoil under condition (A) and (B) in Fig. 4.11

The lee ward side of the airfoil has large negative pressure on the leading edge at moment A and small suction force on the trailing edge of the airfoil. Compared to A, at moment B there is considerable smaller negative pressure on the leading edge of the airfoil and larger suction on the trailing edge of the airfoil. At moment A, since the airfoil is moving from right side to left side and rotating anticlockwise at the same time, the acceleration due to translational movement is the highest. Both the leading edge and the trailing edge rapidly produce a strong vortex sheet.

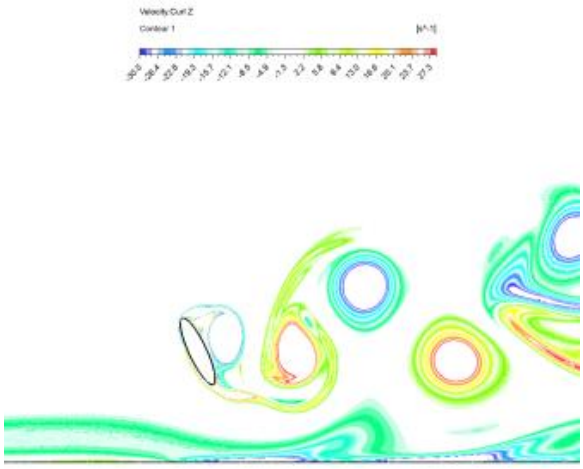

(a)

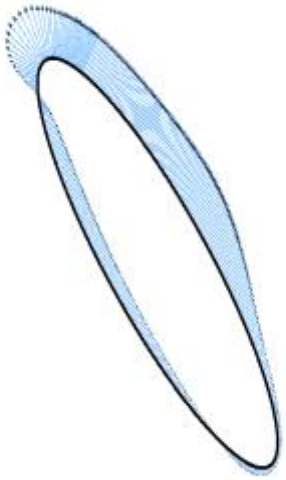

(b)

Figure 5.11 (a) Vortex structure and (b) pressure coefficient around the airfoil in forward flight at H/C=1.5

As the angle of attack is decreases from the position at t=1T/16, the lee side of the foil generates higher negative pressure, which results in the lift contribution from leeward side to increase greatly. Comparing to the hover case at the same moment, there is no “one single vortex LEV-0U” attached to the windward side of the airfoil due to the effect of the incoming flow. Thus, the positive pressure is still high at this position.

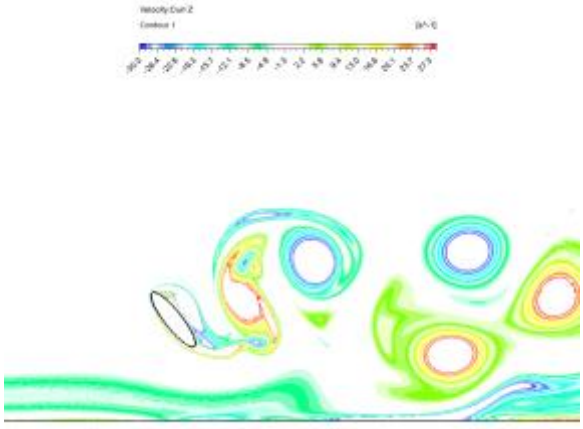

(a)

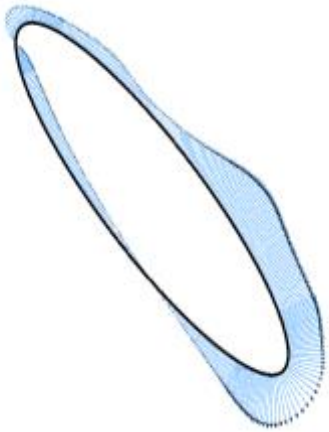

(b)

Figure 5.12 (a) Vortex structure and (b) pressure coefficient around the airfoil in forward flight at H/C=1.5

From 3T/16 to 8T/16, the angle of attack first decreases and then increases. Taking into account the change in angle of attack, lift on leeward side of the airfoil at t=5T/16 reaches the maximum value.

During down stroke the lift coefficient mainly depends on the angle of attack and it varies in time due to the vortex generation and shedding alternatively.

At t=9T/16, the direction of flow is the same as the direction of the airfoil movement and thus the lift is negative. At t=13T/16 the lift becomes lowest due to the angle of attack reaching the highest position. Compared to the hover case, in forward flight, the airfoil does not fly through the vortex formed during the down stroke. Therefore, the enhancement in lift due to the vortex is negligible.

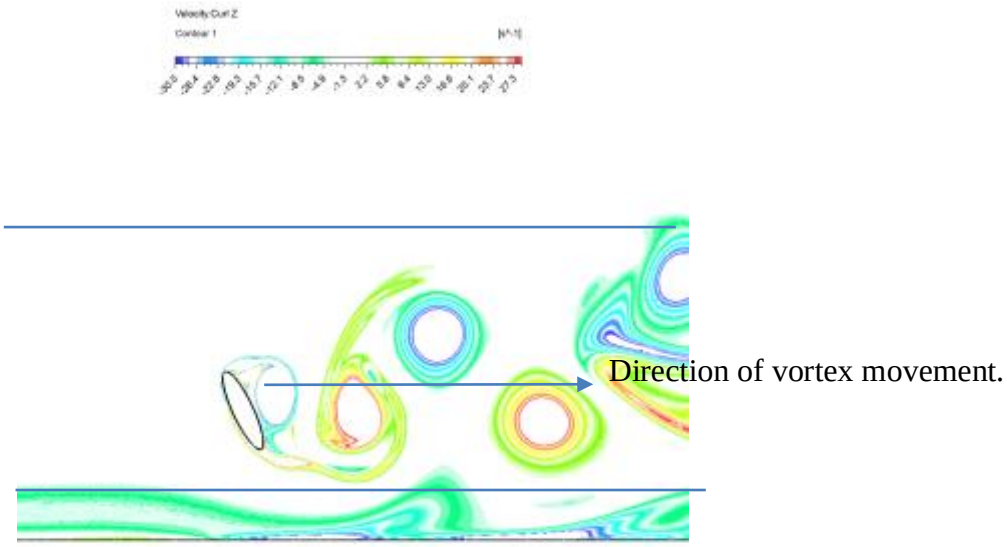

Figure 5.13 Vortex structure in forward flight at H/C=1.5

Compared to the unbounded flow field, at t=1T/16 the lift at H/C=1.5 is larger than that at H/C=5. To show the reason for this behavior, we compare the pressure coefficient distribution around the airfoil. At the same moment, the angle of attack at different height above the ground

is identical. Thus, the suction effect on the leeward of the airfoil is the same. Due to the vortex generated at the leading edge and the trailing edge of the airfoil, the strength of the vortex is not the same and therefore the pressure coefficients in Fig. 5.14 are not identical. From Fig. 5.14 and Fig. 5.15, it can be concluded that because of the ground, the strengths of LEV-1D and TEV-1D at H/C=1.5 are greater than LEV-1D and TEV-1D at H/C=5.

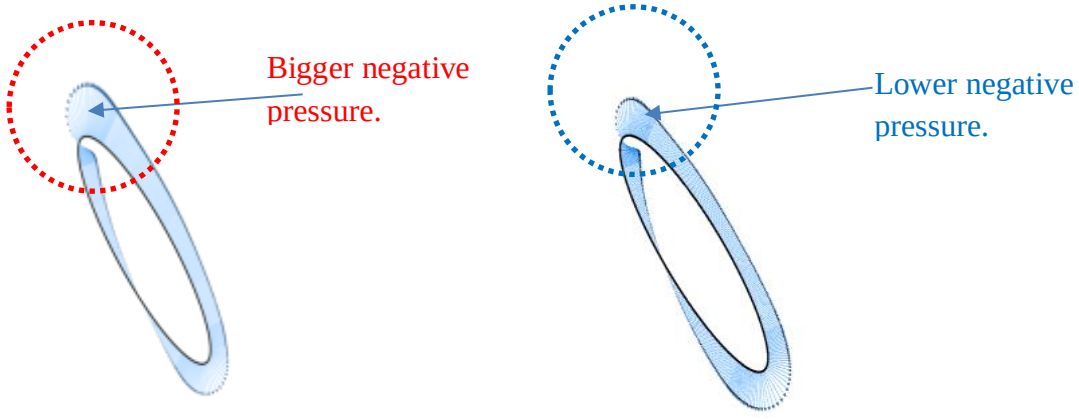

(a) H/C=1.5 (b) H/C=5

Figure 5.14 Pressure coefficients around the airfoil for different height at $t = \frac{3T}{16}$ for H/C=1.5 and 5

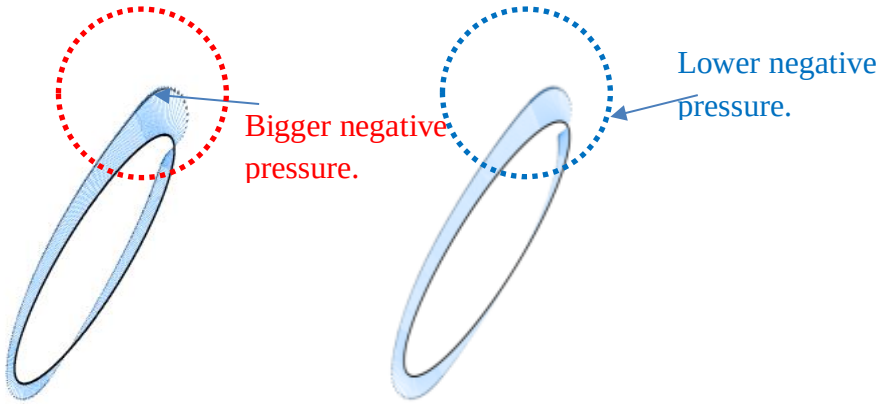

(a) H/C=5 (b) H/C=1.5

Figure 5.15 Pressure coefficients around the airfoil for different height at $t = \frac{13T}{16}$ for H/C=1.5 and 5

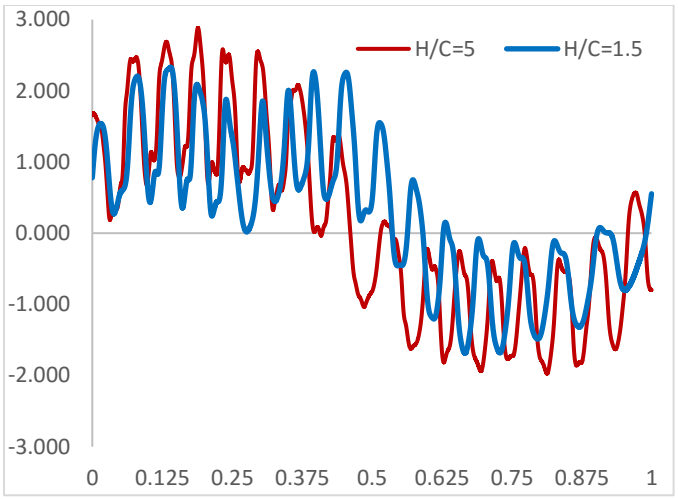

Figure 5.16 Variation in lift coefficients with time during one period in forward flight at H/C=1.5 and H/C=5

For vortex structure D in Fig. 4.11, the area of positive pressure on the wind ward side of the airfoil is bigger than that at H/C=1.5. Since in the up stroke, the LEV-0D stretches the vortex LEV-1D and induces a higher speed bellow the airfoil. LEV-0D also influences the strength of the LEV-1D.

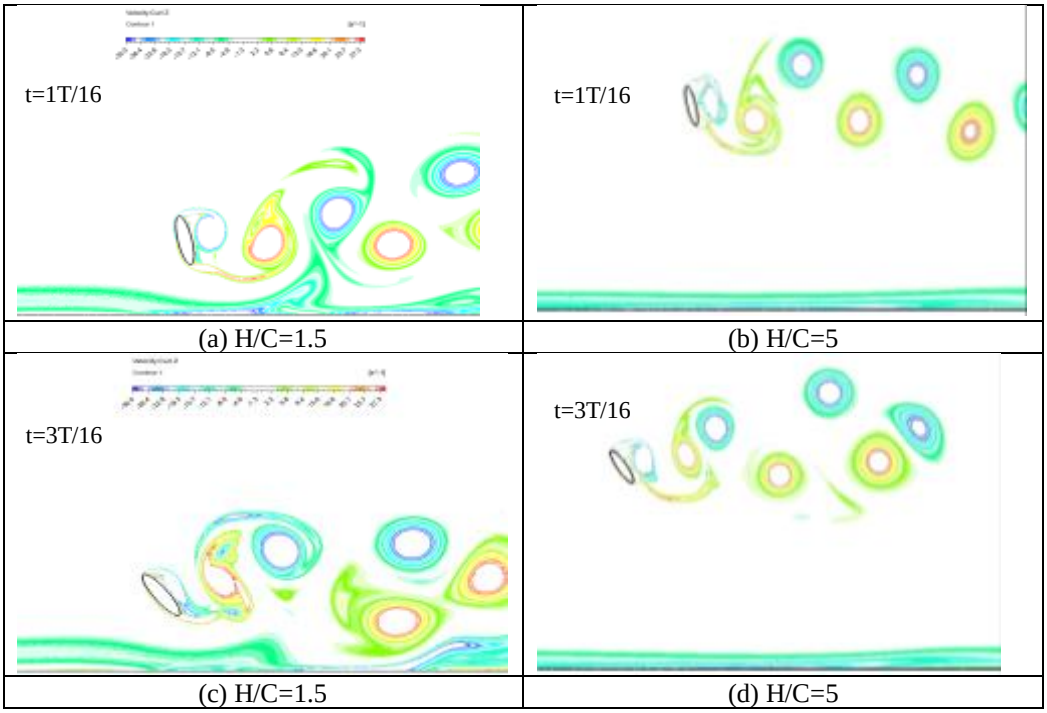

Figure 5.17 Vorticity contours at different heights in forward flight at t=1T/16 and t=3T/16

As the height of the airfoil decreases from the ground, the ground obstructs the flow around the airfoil, which directly affects the vortex structure on the airfoil surface. As comparing the vortex structure at H/C=5 and H/C=1/5 at t= 1T/16 and t=3T/16 shown in Fig. 5.17, it is evident that the vortex interaction with the ground becomes significant at H/C=1.5 which directly changes the vortex structures in the wake. Close to the ground, due to compression of area between the ground and the airfoil flowfield, the vortices are compressed to become oblate. The phenomenon of deformation of vortices to become oblate shape due to the ground leads to change in the flow pattern which further leads to the change in aerodynamic forces.

Chapter 6: Conclusions

In this thesis, the flow fields and the aerodynamic characteristics of a flapping elliptic airfoil in unbounded flow and in ground effect are analyzed by numerical simulations.

In unbounded flow, three-typical vortex structure topologies are obtained due to the translational forces, rotational circulation and wake capture. By comparing the pressure coefficient and vortex structure around the airfoil at three typical instances during hover and forward flight in unbounded flow, the influence of incoming flow on the vortex structure and the flow physics behind the high lift mechanism is analyzed.

In hovering flight in ground effect, as the height of the ground mainly restricts the descent of the leading and trailing edge vortex pair from the airfoil. As the height of the airfoil above the ground decreases, the trailing edge vortex in up-stroke gradually moves to the right away from the airfoil and the resulting changed in the vortex structure lead to increase in lift.

In the forward flight, typical vortex structure due to translational forces and rotational circulation still exist. Due to incoming flow, the vortex generated at the leading edge is shed from the airfoil rapidly. Shedding vortices moving stream-wise with the incoming flow result in a complex vortex street, which leads to the disappearance of wake capture effect on the vortex structure as well as the lift enhancement in upstroke. Close to the ground, due to compression effect, the vortices become oblate. This phenomenon of deformation of vortices to become oblate and enhancement in their strength due to the proximity of the ground leads to significant changes in the aerodynamic forces.

References

1. Shyy, W., Aono, H., Chimakurthi, S. K., Trizila, P., Kang, C.-K., Cesnik, C. E. S., and Liu, H., "Recent Progress in Flapping Wing Aerodynamics and Aeroelasticity," Progress in Aerospace Sciences, Vol. 46, No. 7, 2010, pp. 284-327.

2. Peasavento U. and Wang Z. J., "Flapping Wing Flight Can Save Aerodynamic Power Compared to Steady Flight," Physical Rev. Lett., Vol. 103, 2009, p.118102.

3. Sane, S. P., and Dickinson, M. H., "The Aerodynamic Effects of Wing Rotation and a Revised Quasi-Steady Model of Flapping Flight," Journal of Experimental Biology 205, No. 8, 2002, pp. 1087-1096.

4. Dickinson, M. H., Lehmann, F.-O., and Sanjay, P. S., "Wing Rotation and the Aerodynamic Basis of Insect Flight," Science Vol. 284, No. 5422, 1999, pp. 1954-1960.

5. Mao, Sun. and Tang J., "Unsteady Aerodynamic Force Generation by a Model Fruit Fly Wing in Flapping Motion," Journal of Experimental Biology, Vol. 205, No. 1, 2002, pp. 55-70.

6. Ellington, C. P., "The Novel Aerodynamics of Insect Flight: Applications to Micro-Air Vehicles," Journal of Experimental Biology, Vol. 202, No. 23, 1999, pp. 3439-3448.

7. Gao, T. and Xi-Yun, L., "Insect Normal Hovering Flight in Ground Effect," Physics of Fluids, Vol. 20, No. 8, 2008, P. 087101.

Vita

Hang Li

Degrees M.S. Aerospace Engineering, May 2017

B.S. Aerospace Engineering, June 2014

May 2017